

Received February 12, 2020, accepted February 24, 2020, date of publication February 28, 2020, date of current version March 11, 2020.

Digital Object Identifier 10.1109/ACCESS.2020.2977208

Channel Characterization for Vehicle-to-Infrastructure Communications in Millimeter-Wave Band

DONG YAN^{1,2}, (Student Member, IEEE), KE GUAN^{1,2}, (Senior Member, IEEE),
DANPING HE^{1,2}, (Member, IEEE), BO AI^{1,2}, (Senior Member, IEEE), ZAN LI^{1,2},
JUNHYEONG KIM³, HEESANG CHUNG³, AND
ZHANGDUI ZHONG^{1,2}, (Senior Member, IEEE)

¹State Key Laboratory of Rail Traffic Control and Safety, Beijing Jiaotong University, Beijing 100044, China

²Beijing Engineering Research Center of High-speed Railway Broadband Mobile Communications, Beijing Jiaotong University, Beijing 100044, China

³Moving Wireless Network Research Section, Electronics and Telecommunications Research Institute (ETRI), Daejeon 34129, South Korea

Corresponding author: Ke Guan (kguan@bjtu.edu.cn)

This work was supported in part by the Institute of Information and Communications Technology Planning and Evaluation (IITP) grant funded by the Korean Government (MSIT), QoE Improvement of Open Wi-Fi on Public Transportation for the Reduction of Communication Expense, under Grant 2018-0-00792, and in part by the IITP grant funded by the Korean Government (MSIT) (5G AgiLe and fFlexible integration of SaTellite And cellulaR) under Grant 2018-0-00175.

ABSTRACT In recent years, the intelligent transport system (ITS) has been developed rapidly because of global urbanization and industrialization, which is considered as the key enabling technology to improve road safety, traffic efficiency, and driving experience. To achieve these goals, vehicles need to be equipped with a large number of sensors to enable the generation and exchange of high-rate data streams. Recently, millimeter-wave (mmWave) technology has been introduced as a means of meeting such a high data rate requirement. In this paper, a comprehensive study on the channel characteristics for vehicle-to-infrastructure (V2I) link in mmWave band (22.1-23.1 GHz) for various road environments and deployment configurations is conducted. The self-developed ray-tracing (RT) simulator is employed with the calibrated electromagnetic (EM) parameters. The three-dimensional (3D) environment models are reconstructed from the OpenStreetMap (OSM). In the simulations, not only the vehicle user equipment (UE) moves, but also the other vehicles such as cars, delivery vans, and buses move around the vehicle UE. Moreover, the impacts of the receiver (Rx) multiple antennas and beam switching technologies at the vehicle UE are evaluated as well. The channel parameters of the V2I link in mmWave band, including received power, Rician K -factor, root-mean-square delay spread, and angular spreads are explored in the target scenarios under different simulation deployments. This work aims to help the researchers understand the channel characteristics of the V2I links in mmWave band and support the link-level and system-level design for future vehicular communications.

INDEX TERMS Channel characterization, millimeter-wave communication, ray-tracing simulation, vehicle-to-infrastructure link, wave propagation.

I. INTRODUCTION

The intelligent transport system (ITS) is defined as the set of applications to provide innovative services for the transport of various modes and involve a wide range of different technologies and applications such as beam switching during

The associate editor coordinating the review of this manuscript and approving it for publication was Amjad Mehmood¹.

the overtaking process, dynamic traffic light sequence, and autonomous vehicles [1].

In the ITS, the vehicular Ad-hoc Network (VANET) is envisaged as the most important component to realizing intelligent connected vehicles, which is incorporated in the following architectures: vehicle-to-vehicle (V2V), vehicle-to-infrastructure (V2I), vehicle-to-pedestrians (V2P) and vehicle-to-everything (V2X) [2]. The V2V communications are realized among the moving vehicles i.e., vehicles

act as sources, destinations, and routers in the communication process. Intermediate nodes (vehicles) transfer messages between the source and destination nodes. The V2I communications allow vehicles to communicate with Road Side Units (RSUs). In this case, vehicles act as source and destination [3]. The V2P allows direct, instant, and flexible communication between moving vehicles and roadside passengers. With pocket wireless devices, passengers can easily join the VANETs as roadside nodes and express their travel demands. The V2X provides communication services between a vehicle and networks, vehicles, and pedestrians [4].

Currently, some of the most relevant international standardization bodies like the 3rd Generation Partnership Project (3GPP) and Institute of Electrical and Electronics Engineers (IEEE) 802 have developed their own standards for vehicular communications. In the 3GPP, the enhancements to V2V are mainly studied based on the standardization activities for Long Term Evolution (LTE) V2X [5]. IEEE 802.11p standard is the most important system dedicated to short-range communication. It defines enhancements to 802.11 required to support ITS applications and supports both V2V and V2I communications in the licensed ITS band of 5.9 GHz (5.85-5.925 GHz) [6], [7].

The future V2X services provide the safety-critical vehicular applications (vehicle detection, road detection, lane detection, pedestrian detection, position detection, collision avoidance, etc. [8], [9]) that require ultra-reliability and low latency communications [10]. However, the existing technologies including the aforementioned IEEE 802.11p and LTE-based V2X are unable to meet the requirements of data rate and delay. As the European Commission's Connected-Intelligent Transportation System (C-ITS) has proposed, for the driving becomes more automated and intelligent, the number of sensors (radars, cameras, and Light Detection And Ranging) equipped on each vehicle will be increased. Currently, the number of equipped sensors is around 100, and this number is expected to double by 2020 [11]. With such a large number of sensors, advanced wireless links supporting several multi-Gigabit-per second (Gbit/s) data rates are needed to exchange data from all sensors [12]. Moreover, semi-autonomous and fully autonomous vehicles will require a high rate and low latency communication links to support the applications envisaged by the fifth-generation mobile communications (5G) Infrastructure Public Private Partnership's. These applications include the See-Through use case (maximum latency equal to 50 ms), which enables vehicles to share live video feeds of their onboard cameras to the following vehicles. Other applications such as automated overtaking and high-density platooning are also expected to require communication latencies smaller than 10 ms [11]. Therefore, the wireless industry is moving into the 5G and beyond the 5G era, which can achieve enhanced mobile broadband (eMBB), ultra-reliable and low-latency communications (uRLLC), and massive machine-type communication (mMTC) [13]. This communication system will use the millimeter wave (mmWave)

band, where a large number of spectrum resources are still underutilized, providing unprecedented spectrum and Gbit/s data rates to a mobile device, can support typical cellular communications, vehicular communications, accuracy position, and high-speed-train (HST) communications [14]. The 3GPP focuses on 5G new radio (NR)-based V2I standardization where mmWave is considered to be one of the operating frequencies [15]–[17]. In June 2018, 3GPP TR 37.885 [18] proposed two candidate mmWave carrier frequencies (30 GHz and 63 GHz) for the V2I communications with a recommended bandwidth of 200 MHz. Although there are 60 GHz preliminary propagation measurements in a cellular point-to-point outdoor environment and vehicle scenarios at 28 GHz and 60 GHz [19]–[21], further analysis is still required in more mmWave bands.

In addition, the design of the mmWave technology requires not only received power but also high resolution information in the time and space domains [22]. The location of the antenna and the effects of surrounding objects should be considered and incorporated into the mmWave V2I link. Therefore, it is important to understand the mmWave channel for the V2I communication scenarios. In general, the existing mmWave channel models use traditional frequency band modeling theories and methods, which are divided into two categories: stochastic models and deterministic models [23]. Stochastic models (such as GBSM) use random geometric points to characterize the propagation environment and parameterize them using channel measurement data [24], [25]. However, characterizing the environment with geometric points means simplifying the physical properties of the environment, which also makes it difficult to accurately predict the channel impulse response under certain conditions [26].

The ray-tracing (RT) modeling method is one of the deterministic modeling methods [27] used by the IEEE standard group for mmWave high-speed mobile communication [28]. Compared to stochastic channel modeling, the RT can accurately describe the multipath effects of a given environment model and deployment configuration. It has been successfully applied to different works [29]–[32]. The authors of [29] give the concept of performing the virtual drive test (VDT) by using RT, which is cost-effective and practical. Moreover, the channel parameters extracted from the RT simulation results can be used in the future to design and develop multi-antenna systems. In addition, the authors of [30] analyze the influences of typical objects in rural railway environments at 28 GHz by using the RT simulator. The analysis of RT simulation results and the extraction of channel parameters (including the path loss (PL), root-mean-square (RMS) delay spread (DS), etc.) not only help to understand the important influential factors of the propagation channel at the object level but also guide the deployment of mmWave communication systems. As for now, many research works have shown that RT is not only a powerful tool for deterministic channel modeling, but also a powerful tool for bridging the gap between limited channel measurements and the

requirements for comprehensive parameters by stochastic channel models. However, the computation time of the RT increases with the size of the environment and the number of tasks, and its accuracy depends to a large extent on reliable environmental models and material parameters.

A high-performance cloud-based RT simulation platform (CloudRT) is developed in [33], which is open accessed by “http://raytracer.cloud”. By performing the RT simulation at each frequency point (f_i) to obtain the wideband channel transfer function (CTF) in the whole frequency domain, which is presented as $H(f_i)$. Then, the time domain channel impulse response (CIR) under the corresponding bandwidth is obtained through Inverse fast Fourier transform (IFFT). Based on the CloudRT, the efficiency is significantly improved and a large number of moving scatterers can be added to the scenario, making it suitable for generating reliable channel data to evaluate the mmWave V2I link. In addition, many researchers have performed a large number of works on accurate and effective mmWave dynamic channel measurements in typical application scenarios, such as related work proposed in [34], [35]. These works can be used to calibrate the RT for better accuracy.

Therefore, in this paper, a comprehensive study on the channel characteristics for V2I link in mmWave band (22.1-23.1 GHz) for various road environments and deployment configurations is conducted. The contributions of this work are composed as follows:

- We characterize the mmWave V2I link with consideration of the impact of overtaking and deployment configuration, such as various base station (BS) heights and vehicle initial placements. In the simulations, not only the vehicle user equipment (UE) can move, but also the other vehicles (passenger car, delivery van, and bus) can move around the vehicle UE. Then, we evaluate the impact of the receiver (Rx) multiple antennas and beam switching technologies at the vehicle UE.
- The high-performance cloud-based RT is employed to conduct intensive simulations with massive mobile vehicles. Our previous works calibrate and provide electromagnetic (EM) parameters in this region for realistic RT simulations [3], [36], [37]. The three-dimensional (3D) model of the selected area is reconstructed from the OpenStreetMap (OSM). The received power, RMS delay spread, Rician K -factor (KF), and angular spreads are analyzed and compared between different configurations. The analysis and the provided parameters in this paper will help researchers understand the propagation channel for designing mmWave V2I communication systems.

The rest of this paper is organized as follows: In section II, the measurement campaigns and RT validation are introduced. Section III introduces the urban and highway scenarios and the simulation configurations. In Section IV, all the channel parameters of the mmWave V2I link are characterized and summarized for the urban and highway scenarios, respectively. Finally, conclusions are drawn in Section V.

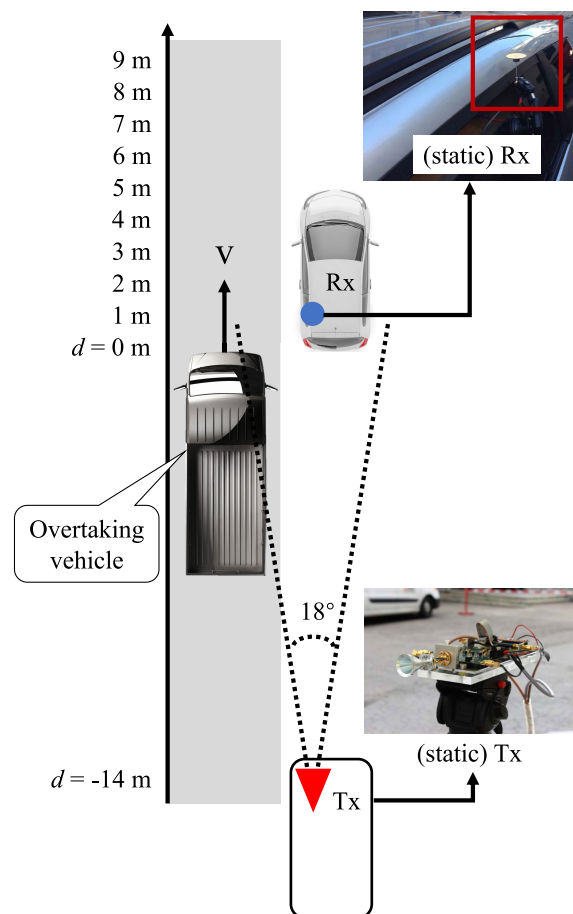


FIGURE 1. Bird’s-eye view of the measurement campaign which is from [38]. Both Tx and Rx are static. The overtaking vehicle moves at an excess speed v relative to the static vehicles.

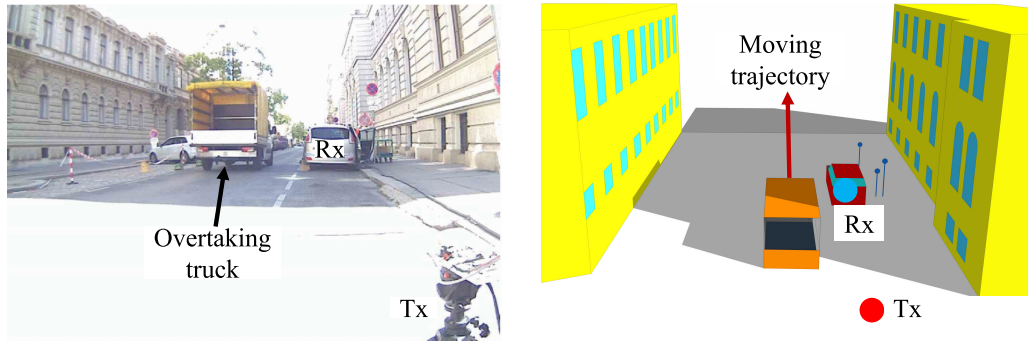
II. CHANNEL MEASUREMENT AND RT SIMULATION

In this section, by comparing the results obtained from the measurement campaign in [38] and the simulation results obtained through the RT simulator under the same environments, the accuracy of the RT simulator is verified.

A. MEASUREMENT CAMPAIGN

The measurement campaign in [38] analyzes the effect of an overtaking vehicle on the mmWave V2V wideband channel, which is conducted in an urban street in the center of Vienna, Austria. The setup for measurement is to simulate the scenario of two cars driving in the same direction with a constant distance, then the third vehicle overtakes this car platoon.

For the measurement, a custom-built omni-directional ($\lambda/4$) monopole antenna is used as the Rx. As shown in Fig. 1, the Rx is deployed on the left window of the static car in the front. The transmitter (Tx) is a horn antenna with an 18° half-power beamwidth, which is aligned towards the Rx car. During the measurement, Tx and Rx are both with a height of 1.56 m and the Tx is approximately 15 m behind the Rx. Due to the Tx is a directive horn antenna, the single reflection at the Tx car can be ignored. In addition, high order



(a) Measurement scenario in an urban street, which is from [38].

(b) The reconstructed 3-D environment model

FIGURE 2. Comparison of the measurement scenario and the RT simulation scenario. (a) Measurement scenario in an urban street, which is from [38]. (b) The reconstructed 3-D environment model.

reflections are below the Rx sensitive. Therefore, the Tx car is replaced by a simple tripod mounting. Then the effect of overtaking vehicles can be analyzed with excess speeds of up to 13 m/s. In Fig. 1, the distance “d” represents the “bumper to bumper distance”, which means the distance between the front bumper of the overtaking vehicle and the rear bumper of the static Rx car. The reference plane is the position where “d = 0 m”. The considered measurement range varies from d = 1 m to 9 m and is marked on the left-hand side in the figure. The channel sounder was operated at 60 GHz with 510 MHz bandwidth. More details about the measurement campaign such as “frequency synchronization, time synchronization, measurement data memorize and processing” can be found in [38].

B. VALIDATION OF RT SIMULATOR

The 3D environment model in Fig. 2 is reconstructed according to the measurement campaign and measurement scenario. The parked car, ground, and significant objects such as traffic signs, are considered in the model. The geometry of the RT simulation scenario is the same as the measurement scenario. The antenna locations and patterns in the simulation are the same as the aforementioned in the measurement. The Tx power is set to 0 dBm, in order to eliminate the system influence. Then the extensive RT simulations are conducted at the center frequency 60 GHz with 510 MHz bandwidth. The number of frequency points is 103, which is the same as the number of sub-carriers in the measurement. For the propagation mechanisms, the line-of-sight (LOS) ray, reflected rays (up to the 2nd order) and scattered rays are considered in the simulations, which can balance the simulation accuracy and the computational complexity.

In the simulation, we selected the truck as an overtaking vehicle. The moving trajectory can be seen in Fig. 2 and the distance interval of each snapshot is 0.25 m. Through comparing the position-specific relative LOS tap gain and RMS delay spread between measurement results and RT simulation results, the accuracy of our RT simulator can

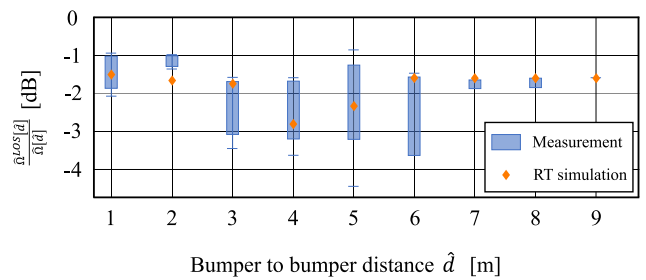


FIGURE 3. Box plot of the position-specific relative LOS tap gain.

be verified. The position-specific relative LOS tap gain means the strength of the LOS delay tap relative to all taps at the specific positions, which is represented by $\hat{\Omega}^{LOS}[\hat{d}]/\hat{\Omega}[\hat{d}]$. Both the strength of the LOS delay tap ($\hat{\Omega}^{LOS}[\hat{d}]$) and the strength of all taps ($\hat{\Omega}[\hat{d}]$) in the measurement results are distance-dependent estimated values. The distance interval in the measurement is 0.25 m. For the sake of illustration, the measurement results of each sampling point are rounded to the nearest integer meter value, and then drawn into a box plot on a meter based grid. As shown in Fig. 3 and Fig. 4, the bottom and top edges of the box indicate the 25th and 75th percentiles. The whiskers show the 5th and 95th percentiles.

We use the same data processing method to the simulation results, where simulation results of each sampling point are rounded to the nearest integer meter value. Each integer meter will thus include several rounded samples, from which a median value can be calculated. In total, 9 median values can be obtained. Then the median values are represented by the yellow diamond in Fig. 3.

In addition, the RMS delay spread can be calculated by:

$$\sigma_{\tau} = \sqrt{\frac{\sum_{n=1}^N \tau_n^2 \cdot P_n}{\sum_{n=1}^N P_n} - \left(\frac{\sum_{n=1}^N \tau_n \cdot P_n}{\sum_{n=1}^N P_n} \right)^2} \tag{1}$$

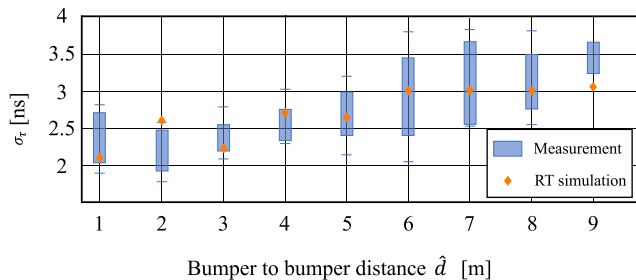


FIGURE 4. Box plot of the RMS delay spread.

where σ_τ denotes the RMS delay spread, P_n and τ_n denote the power and the excess delay of the n -th tap, respectively. Using a similar data processing method, the RMS delay spread is compared in Fig. 4.

The comparison between simulation results and the measurement results is shown in Fig. 3 and Fig. 4, respectively. In most cases, the simulation results are within the ranges of the measurement results, which are denoted by the boxes and whiskers. Matching the simulation results to the measurement results well verifies the accuracy of the propagation mechanism model and material EM parameters in our RT simulator. Moreover, the accuracy of interactions between typical structures (such as buildings, ground, traffic signs, etc.) can be validated. Therefore, the simulator can be used for channel simulation under similar scenarios with similar materials and the simulation results can be used to channel characteristic analysis, such as the measurement campaigns in the reference [39]. However, in some positions, the simulation results cannot map the measurement result very well. It is mainly due to the inaccuracy of the 3D digital map, which will cause some differences between the simulation scenario and the measurement scenario.

III. RT SIMULATIONS FOR THE V2I LINK IN URBAN AND HIGHWAY SCENARIOS

In this section, the simulation scenarios of typical urban and highway are defined and reconstructed. For both the urban and the highway scenarios, the Rx is always deployed on the bus, which represented as the vehicle UE in the following part. We also considered different traffic flow (full/low traffic flow) for all the cases. Moreover, not only the various heights of the BS are considered, but also the impact on different overtaking situations are in the consideration. For the different overtaking situations (the vehicle UE overtakes the bus and the vehicle UE overtakes the car), the multiple antennas and beam switching technologies at the vehicle UE are also considered. Thus, a total of 44 cases are simulated (sampling interval: 0.83 m both in the urban scenario and highway scenario, respectively), which are listed in Table 5. The details for simulation configurations are as follows.

A. OVERVIEW OF SCENARIOS

1) URBAN SCENARIO

The RT simulations are realized by the reconstructed 3D environment model with calibrated EM parameters. Based on the

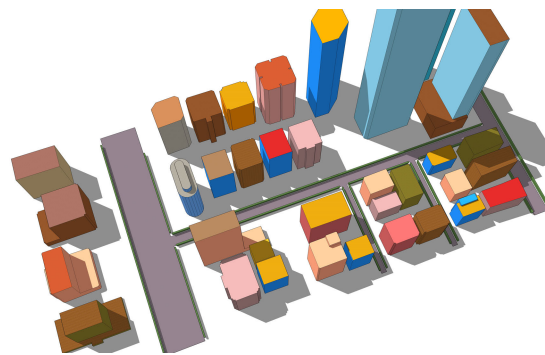


FIGURE 5. 3D model of the constructed urban scenario in Seoul.

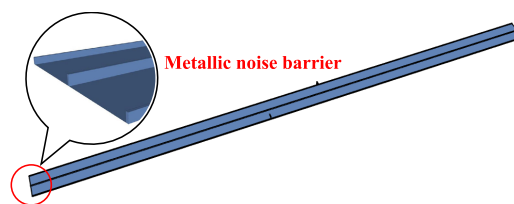


FIGURE 6. 3D model of the constructed highway scenario.

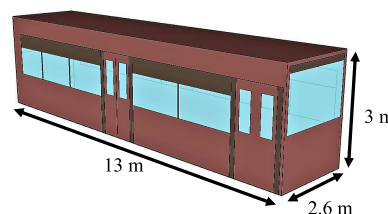


FIGURE 7. 3D model of the bus in the simulation.

OSM, which is a collaborative project to create a free editable map of the world, the 3D details of the considered environment are obtained. With a self-developed plugin (available on <http://www.raytracer.cloud/software>), the OSM data can be directly imported to the SketchUp, which is a widely used 3D modeling computer program for drawing applications such as architecture (more details about SketchUp can be found on <https://www.sketchup.com/>). Then, the 3D environment model for the RT simulation can be generated. In this work, one typical urban street with 4 lanes in Seoul is selected as the simulation scenario (see Fig. 5).

2) HIGHWAY SCENARIO

As shown in Fig. 6, an 8-lane highway is reconstructed by the SketchUp, with the concrete guardrail in the middle and the metallic noise barrier on both sides of the highway.

B. VEHICLE TYPES AND VEHICLE INITIAL PLACEMENTS

In this study, different vehicle types and vehicle initial placements are considered in both the urban and highway scenarios. Based on the 3GPP TR 37.885 [18], three vehicle types and the distribution of each kind of vehicle are clarified in Table 1. The 3D models of each vehicle type are shown in Fig. 7 - Fig. 9.

TABLE 1. Vehicle types in the simulation and distribution.

Vehicle type	Length	Width	Height	Percentage of the total vehicle
Bus	13 m	2.6 m	3 m	20%
Passenger car	5 m	2 m	1.6 m	60%
Delivery van	13.5 m	2.6 m	3.5 m	20%

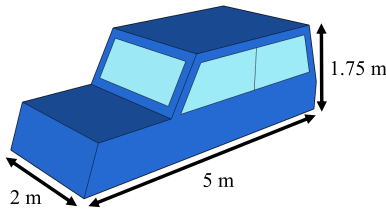


FIGURE 8. 3D model of the passenger car in the simulation.

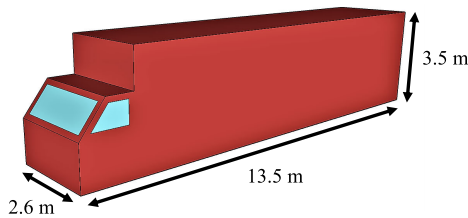


FIGURE 9. 3D model of the delivery van in the simulation.

Moreover, the vehicles are placed in the urban and highway scenarios according to the following process:

- The distance between the rear bumper of a vehicle and the front bumper of the following vehicle in the same lane is $\max \{2, x \cdot 2 \text{ sec}\} \text{ m}$, where x is a realization of an exponential random variable with the average of the speed.
- All the vehicles in the same lane have the same speed.
- Vehicle type distribution is not dependent of the lane.

In both the urban and the highway scenarios, the vehicles in each lane are randomly generated according to vehicle distribution. The vehicles do not change direction at the intersection and the speed in each lane is marked in Fig. 10 and Fig. 11.

C. SIMULATION CONFIGURATION

In the simulations, the carrier frequency is 22.6 GHz with a bandwidth of 1 GHz. The Rx beam pattern is the same as the Tx antenna beam pattern (see Fig. 12). To explore the impact of the beam switching technologies at the vehicle UE, the Tx beam is fixed, and the multiple antennas at the vehicle UE are placed on the top of the bus head with a height of 3.2 m (bus height: 3 m). These three beams have the same pattern and the beamwidth of the main lobe is around 20°, therefore, each of which has a 20° to another (see Fig. 13).

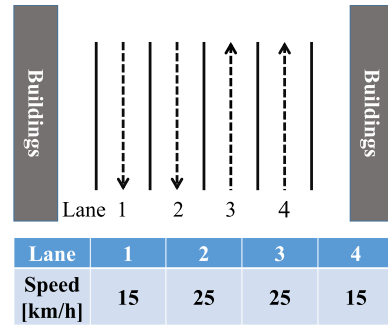


FIGURE 10. 4-lane road in the urban scenario.

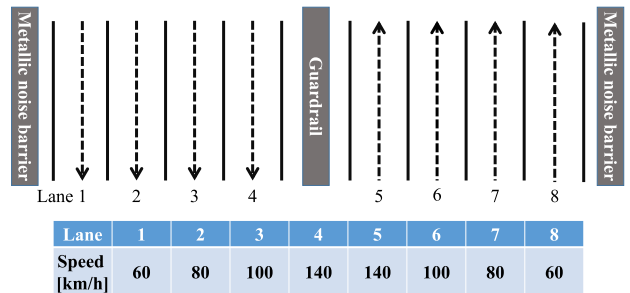


FIGURE 11. 8-lane road in the highway scenario.

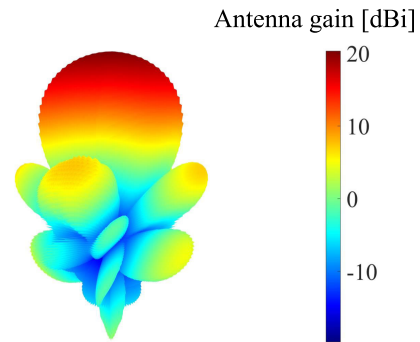


FIGURE 12. Tx and Rx antenna pattern in the simulation.

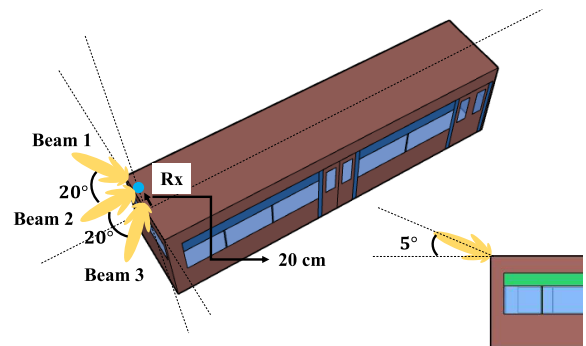


FIGURE 13. Location of multiple antennas at the vehicle UE.

For the overtaking situation in the urban scenario, the Tx is placed in a building on the roadside with $(x, y, z) = (182, 38, 25)$, with the main lobe pointing at $(x, y, z) = (500, 0, 0)$. The vehicle UE is driven in lane 1 at

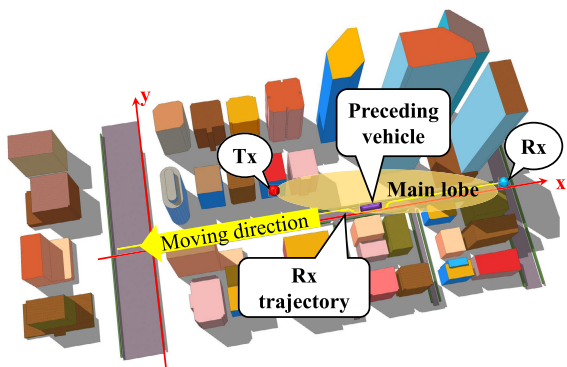


FIGURE 14. Overtaking situation in the urban scenario.

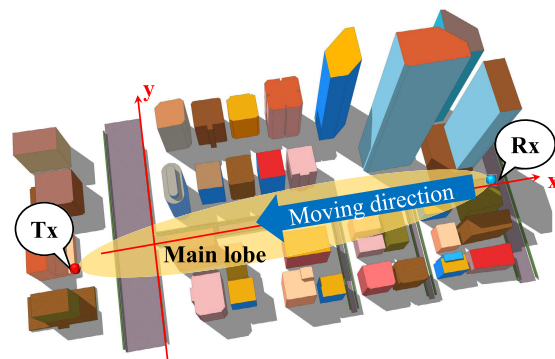


FIGURE 16. Various BS heights in the urban scenario.

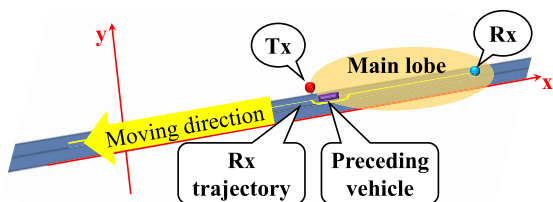


FIGURE 15. Overtaking situation in the highway scenario.

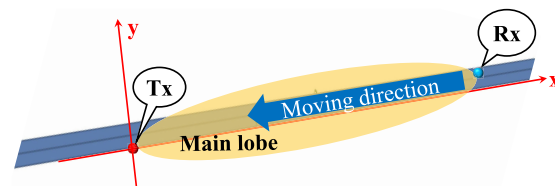


FIGURE 17. Various BS heights in the highway scenario.

a speed 15 km/h, then the vehicle UE gradually returns to the fast lane at the point of (415, 7, 0). After overtaking the preceding vehicle at the point of (330, 3.5, 0), the vehicle UE comes back to lane 1 (see Fig. 14).

For the overtaking situation in the highway scenario, as shown in Fig. 15, the Tx is located above the traffic light and the corresponding coordinates are (340, 35, 10). The main lobe of the Tx is pointing at (500, 17, 0). The trajectory of the vehicle UE in the highway scenario is similar to the trajectory in the urban scenario. The only difference is that the vehicle UE in the highway scenario changes from lane 3 to lane 4 to complete the overtaking process.

In the case of “various BS heights” for both urban and highway scenarios, the moving distance of the vehicle UE is 500 m and the main lobe of the Tx is pointing at (500, 0, 0). The Tx is placed next to a building in the urban scenario (see Fig. 16) and by the roadside in the highway scenario (see Fig. 17) with the height varying from 5 m to 25 m.

Table 2 summarizes the locations and heights of the Tx and Rx in the both “overtaking situation” and “various BS heights” cases. The simulation configurations for all the cases are concluded in Table 3.

In the case of the “overtaking situation”, we evaluate the multiple antennas and beam switching (Beam 1, 2, 3) techniques at the Rx; for the “various BS heights”, we mainly study the impact of different BS heights on beam 2. For the propagation mechanisms, direct, reflection, scattering, diffraction and transmission are considered.

The EM parameters of the involved materials have been calibrated in our preliminary work [40]–[43] and are summarized in the Table 4, where ϵ_r' is the real part of the relative

TABLE 2. The locations and heights of the Tx and Rx.

Transceiver	Case	Scenario	
		Urban	Highway
Tx	Overtaking Situation	Placed in a building on the roadside (182,38,25)	Placed above the traffic light (340,35,10)
	Various BS Heights	Next to the building (-80,-23,z), z=5,10,15, 20,25	By the roadside (0,-5,z), z=5,10,15, 20,25
Rx	Overtaking Situation	Placed on the top of the bus with a height of 3.2m	
	Various BS Height		

permittivity, $\tan\delta$ is the loss tangent, S and α are the scattering coefficient and scattering exponent of the directive scattering model [44]. Therefore, with the provided calibrated parameters, we can further conduct RT simulations with various Tx/Rx deployments.

D. RT SIMULATIONS FOR DIFFERENT CASES

For both the urban and the highway scenarios, besides considering the multiple antennas and beam switching (Beam 1, 2, 3) at the vehicle UE in the different overtaking situations mentioned above and various BS heights, we have additionally considered two different traffic flows:

- Full traffic flow: all the randomly generated vehicles on the road
- Low traffic flow: 10% of all the randomly generated vehicles on the road

TABLE 3. Simulation configuration for urban and highway scenarios.

Frequency range	22.1-23.1 GHz	
Frequency step	0.3 MHz	
Antenna type	Directional antenna	
Tx	Power	20 dBm
	Maximum antenna gain	16 dBi
Rx	Angle between the three beams	20 degree
	Maximum antenna gain	16 dBi
Propagation mechanism	LOS	✓
	Reflection	up to 2 nd order
	Scattering	Directive scattering model
	Diffraction	Deygout
	Transmission	✓
Material	Building	Brick, Mable, Thoughglass
	Urban furniture, Vehicle	Metal
	Tree	Wood
	Ground, Highway guardrail	Concrete

TABLE 4. EM parameters of different materials.

Material	ϵ_r'	$\tan\delta$	S	α
Brick	1.9155	0.0568	0.0019	49.5724
Marble	3.0045	0.2828	0.0022	15.3747
Thoughglass	1.0538	23.9211	0.0025	5.5106
Metal	1	10 ⁷	0.0026	17.7691
Concrete	5.4745	0.0021	0.0011	109
Wood	6.6	0.9394	0.0086	13.1404

Hence, a total of 44 cases are considered in this work, which is summarized in Table 5 for clarity. U and H stand for urban and highway scenarios, respectively. Overtaking is represented by OT, while traffic flow is represented by TF, respectively.

IV. KEY CHANNEL PARAMETERS FOR EXTENSIVE SIMULATIONS

Based on extensive RT simulation results, the mmWave V2I channel in urban and highway scenarios with two cases (“overtaking situation” and “various BS heights”) are characterized by the following relevant parameters: received power, RMS delay spread, KF, azimuth angular spread of arrival (ASA), azimuth angular spread of departure (ASD), elevation angular spread of arrival (ESA) and elevation angular spread of departure (ESD).

All these channel parameters are fitted by the normal distribution with the mean value μ and the standard deviation (STD) σ . However, in some cases, the fitting results performance not well. This is due to the relatively large travel distance of the vehicle UE and the moving scatters around the vehicle UE, the channel characteristics may change significantly along the path. Thus, for these cases, it is not suitable to use the log-norm fitting method. The extracted parameters

TABLE 5. Total cases in the simulation.

Situation	Scenario	OT Type	TF	Rx Beam	Tx Height	Case
OT Situation	Urban	Bus	Full	1	25 m	U - OT Bus - TF Full - Beam1
				2		U - OT Bus - TF Full - Beam2
				3		U - OT Bus - TF Full - Beam3
			Low	1		U - OT Bus - TF Low - Beam1
				2		U - OT Bus - TF Low - Beam2
				3		U - OT Bus - TF Low - Beam3
		Car	Full	1		U - OT Car - TF Full - Beam1
				2		U - OT Car - TF Full - Beam2
				3		U - OT Car - TF Full - Beam3
			Low	1		U - OT Car - TF Low - Beam1
				2		U - OT Car - TF Low - Beam2
				3		U - OT Car - TF Low - Beam3
	Highway	Bus	Full	1	10 m	H - OT Bus - TF Full - Beam1
				2		H - OT Bus - TF Full - Beam2
				3		H - OT Bus - TF Full - Beam3
			Low	1		H - OT Bus - TF Low - Beam1
				2		H - OT Bus - TF Low - Beam2
				3		H - OT Bus - TF Low - Beam3
		Car	Full	1		H - OT Car - TF Full - Beam1
				2		H - OT Car - TF Full - Beam2
				3		H - OT Car - TF Full - Beam3
			Low	1		H - OT Car - TF Low - Beam1
				2		H - OT Car - TF Low - Beam2
				3		H - OT Car - TF Low - Beam3
Various BS Heights	Urban	-	Full	2	5 m	U - TF Full - Tx 5~25
				10 m		
				15 m		
				20 m		
				25 m		
				25 m		
	Highway		Full	2	5 m	H - TF Full - Tx 5~25
				10 m		
				15 m		
				20 m		
				25 m		
				25 m		
Urban	-	Low	Full	2	5 m	U - TF Low - Tx 5~25
				10 m		
				15 m		
				20 m		
				25 m		
				25 m		
Highway		Low	Full	2	5 m	H - TF Low - Tx 5~25
					10 m	
					15 m	
					20 m	
					25 m	
					25 m	

are summarized in Table 6 - Table 8, where $\mu_{DS}, \mu_{KF}, \mu_{ASA}, \mu_{ASD}, \mu_{ESA}, \mu_{ESD}$ are the mean values of DS, KF, ASA, ASD, ESA, and ESD, respectively. $\sigma_{DS}, \sigma_{KF}, \sigma_{ASA}, \sigma_{ASD}, \sigma_{ESA}, \sigma_{ESD}$ are the standard deviations of DS, KF, ASA, ASD, ESA, and ESD, respectively. In order to clarify the channel characteristics for these two cases in both urban and highway scenarios, we first study the impact of the overtaking situation and then study the impact of the various BS heights.

A. RECEIVED POWER

1) OVERTAKING SITUATION

The received power in the overtaking situation for both the urban and the highway scenarios (listed in Table 5) are shown in Fig. 18 - Fig. 19.

For all the cases, the blue dotted lines represent the received power of the beam 1, the red dotted lines show the received power of the beam 2 and the green dotted lines indicate the received power of the beam 3.

In the urban scenario, the overtaking process takes place after the snapshot 100 and ends the overtaking process after the snapshot 210 for two different overtaking situations (“vehicle UE overtakes the bus” and “vehicle UE overtakes the passenger car”). In the highway scenario, the overtaking process takes place between snapshot 130 and snapshot 260 for two different overtaking situations.

TABLE 6. Extracted parameters for the DS of overtaking situation and various BS heights.

Case	DS [ns]		Case	DS [ns]	
	μ_{DS}	σ_{DS}		μ_{DS}	σ_{DS}
U - OT Bus - TF Full - Beam1	36.5390	42.4552	H - OT Bus - TF Full - Beam1	22.0043	21.5227
U - OT Bus - TF Full - Beam2	34.3678	33.6972	H - OT Bus - TF Full - Beam2	22.2320	21.4742
U - OT Bus - TF Full - Beam3	71.7180	83.0210	H - OT Bus - TF Full - Beam3	21.9675	20.5944
U - OT Bus - TF Low - Beam1	36.9007	42.9970	H - OT Bus - TF Low - Beam1	6.0409	5.3926
U - OT Bus - TF Low - Beam2	34.8366	34.0699	H - OT Bus - TF Low - Beam2	6.4242	5.1349
U - OT Bus - TF Low - Beam3	72.4428	84.3223	H - OT Bus - TF Low - Beam3	7.2383	4.9227
U - OT Car - TF Full - Beam1	36.1496	42.5777	H - OT Car - TF Full - Beam1	22.8277	22.2697
U - OT Car - TF Full - Beam2	33.8113	33.5094	H - OT Car - TF Full - Beam2	23.0292	22.1775
U - OT Car - TF Full - Beam3	71.0677	82.5418	H - OT Car - TF Full - Beam3	22.7335	21.3301
U - OT Car - TF Low - Beam1	36.3478	42.9794	H - OT Car - TF Low - Beam1	6.1042	5.5062
U - OT Car - TF Low - Beam2	34.3383	34.1668	H - OT Car - TF Low - Beam2	6.4281	5.3013
U - OT Car - TF Low - Beam3	72.2972	83.7287	H - OT Car - TF Low - Beam3	7.2742	5.0835
U - TF Full - Tx 5	3.4421	11.5788	H - TF Full - Tx 5	1.0271	0.4658
U - TF Full - Tx 10	20.8773	28.2027	H - TF Full - Tx 10	1.0529	0.4672
U - TF Full - Tx 15	22.3873	27.9703	H - TF Full - Tx 15	1.0504	0.4672
U - TF Full - Tx 20	36.6491	45.4339	H - TF Full - Tx 20	1.0602	0.4710
U - TF Full - Tx 25	33.9034	38.3102	H - TF Full - Tx 25	1.0495	0.4992
U - TF Low - Tx 5	0.1698	0.3131	H - TF Low - Tx 5	0.4911	0.3676
U - TF Low - Tx 10	20.9909	28.2145	H - TF Low - Tx 10	0.5061	0.3686
U - TF Low - Tx 15	22.6852	27.5801	H - TF Low - Tx 15	2.6015	0.6212
U - TF Low - Tx 20	32.2179	38.8925	H - TF Low - Tx 20	0.5040	0.3643
U - TF Low - Tx 25	29.4885	32.7432	H - TF Low - Tx 25	0.5381	0.4015

TABLE 7. Extracted parameters for the KF of overtaking situation and various BS heights.

Case	KF [dB]		Case	KF [dB]	
	μ_{KF}	σ_{KF}		μ_{KF}	σ_{KF}
U - OT Bus - TF Full - Beam1	12.4682	8.8180	H - OT Bus - TF Full - Beam1	18.8873	15.6428
U - OT Bus - TF Full - Beam2	8.6693	9.5600	H - OT Bus - TF Full - Beam2	18.5657	16.2077
U - OT Bus - TF Full - Beam3	8.2745	7.8493	H - OT Bus - TF Full - Beam3	17.4105	14.6708
U - OT Bus - TF Low - Beam1	12.6453	8.7963	H - OT Bus - TF Low - Beam1	19.9337	10.0417
U - OT Bus - TF Low - Beam2	8.7826	9.4990	H - OT Bus - TF Low - Beam2	17.9215	10.8677
U - OT Bus - TF Low - Beam3	8.2827	7.9971	H - OT Bus - TF Low - Beam3	15.9310	11.7907
U - OT Car - TF Full - Beam1	12.5154	9.3997	H - OT Car - TF Full - Beam1	17.3556	14.6168
U - OT Car - TF Full - Beam2	8.7567	9.4293	H - OT Car - TF Full - Beam2	16.6051	15.2129
U - OT Car - TF Full - Beam3	7.9266	7.9959	H - OT Car - TF Full - Beam3	15.9963	14.0557
U - OT Car - TF Low - Beam1	13.0046	9.5320	H - OT Car - TF Low - Beam1	20.3004	10.3206
U - OT Car - TF Low - Beam2	9.0379	9.4730	H - OT Car - TF Low - Beam2	18.5669	11.5694
U - OT Car - TF Low - Beam3	8.2990	7.8453	H - OT Car - TF Low - Beam3	17.0552	12.5368
U - TF Full - Tx 5	38.5985	14.1390	H - TF Full - Tx 5	40.6512	15.3772
U - TF Full - Tx 10	33.8146	12.9039	H - TF Full - Tx 10	40.4171	15.2836
U - TF Full - Tx 15	27.6064	11.5648	H - TF Full - Tx 15	40.3273	15.3091
U - TF Full - Tx 20	22.3674	13.7122	H - TF Full - Tx 20	40.2364	15.0067
U - TF Full - Tx 25	21.8104	13.2386	H - TF Full - Tx 25	34.6749	18.6632
U - TF Low - Tx 5	40.4160	11.6053	H - TF Low - Tx 5	36.7317	25.4603
U - TF Low - Tx 10	32.3108	16.6020	H - TF Low - Tx 10	30.6577	22.4289
U - TF Low - Tx 15	26.7299	11.2816	H - TF Low - Tx 15	7.0491	5.8198
U - TF Low - Tx 20	16.0792	13.0635	H - TF Low - Tx 20	36.1167	24.0577
U - TF Low - Tx 25	13.8741	10.6733	H - TF Low - Tx 25	19.2189	21.6640

As shown in Fig. 18 and Fig. 19, for all the cases, the received power of beam 2 (represented by the red dotted line) is greater than that of beam 1 (represented by the blue dotted line) before the overtaking process occurs. However, take the overtaking situation in the urban scenario as an example, we can find that, when the overtaking process starts, the vehicle UE gradually turns from lane 1 to lane 2. During this process, with the steering of the vehicle UE, the main lobe

of the beam 2 gradually deviates from the main lobe of the BS, meanwhile, the main lobe of the beam 1 gradually aligns to the main lobe of the BS (see Fig. 20). Therefore, the received power of beam 1 gradually exceeds beam 2.

When the vehicle UE continues to drive in lane 2 and is close to the BS, since the beam 1 is gradually aligned with the main lobe of the BS, and the beam 2 gradually deviates from the main lobe of the BS, the received power of the beam

TABLE 8. Extracted parameters for the ASDs of overtaking situation and various BS heights.

Case	ASD [°]		ESD [°]		ASA [°]		ESA [°]	
	μ_{ASD}	σ_{ASD}	μ_{ESD}	σ_{ESD}	μ_{ASA}	σ_{ASA}	μ_{ESA}	σ_{ESA}
U - OT Bus - TF Full - Beam1	29.6854	17.1734	10.7413	12.6190	41.1988	52.6222	7.4289	7.5972
U - OT Bus - TF Full - Beam2	36.5541	20.6203	11.8913	14.5606	60.1475	45.1646	9.9906	10.1093
U - OT Bus - TF Full - Beam3	39.0820	21.6850	17.4028	21.8023	41.9010	30.9569	11.3004	8.1566
U - OT Bus - TF Low - Beam1	29.7893	17.2189	10.7752	12.5779	40.2625	51.9706	7.0482	7.2618
U - OT Bus - TF Low - Beam2	36.6853	20.6511	11.9803	14.5981	60.0077	45.1602	9.1622	9.2225
U - OT Bus - TF Low - Beam3	39.0801	21.8580	17.4337	21.6795	42.2285	30.8839	10.6151	7.1337
U - OT Car - TF Full - Beam1	29.5393	17.2948	10.8208	12.9941	39.7093	51.1504	7.8835	8.5943
U - OT Car - TF Full - Beam2	36.0328	20.4876	11.7098	14.2608	58.0021	44.3430	10.9530	11.3622
U - OT Car - TF Full - Beam3	38.9180	21.4413	17.0625	21.1263	42.6349	30.6854	12.2839	9.0736
U - OT Car - TF Low - Beam1	29.4573	17.2310	10.6872	12.5725	38.5159	50.5211	7.0206	7.6448
U - OT Car - TF Low - Beam2	36.3895	20.7109	11.9121	14.6145	57.8037	45.0818	9.1587	9.2565
U - OT Car - TF Low - Beam3	39.2538	21.6535	17.3677	21.5004	42.7143	30.8111	10.8208	7.3016
H - OT Bus - TF Full - Beam1	3.2606	4.5523	6.0257	6.2718	81.7504	69.9353	17.4320	16.0032
H - OT Bus - TF Full - Beam2	3.7787	8.3714	6.1297	6.2534	66.0722	49.9345	17.4049	16.3187
H - OT Bus - TF Full - Beam3	4.1100	9.7262	6.1081	5.9815	42.2137	30.2077	15.3087	13.2517
H - OT Bus - TF Low - Beam1	7.6097	14.1637	1.5147	1.2929	80.0742	63.2465	9.2025	5.8879
H - OT Bus - TF Low - Beam2	12.7905	25.7279	1.7173	1.2230	73.9423	41.9639	7.9387	4.7416
H - OT Bus - TF Low - Beam3	15.0183	30.2887	2.1549	1.6425	42.9626	24.9008	8.8575	4.2467
H - OT Car - TF Full - Beam1	10.3910	14.1460	7.2045	7.2185	81.7701	60.9103	17.4746	15.6523
H - OT Car - TF Full - Beam2	11.3458	16.7719	7.3101	7.1938	69.0216	45.1148	17.5141	15.5401
H - OT Car - TF Full - Beam3	12.2655	18.9611	7.2548	6.8746	43.5226	27.3875	15.2632	12.9486
H - OT Car - TF Low - Beam1	10.3633	16.9250	1.5025	1.2683	78.8422	58.5951	9.2997	5.9427
H - OT Car - TF Low - Beam2	13.1511	23.1223	1.6465	1.2505	72.5187	41.6433	7.9925	4.7520
H - OT Car - TF Low - Beam3	14.9588	26.9360	2.0774	1.6856	42.6919	24.2620	8.9514	4.2647
U - TF Full - Tx 5	0.1871	0.7794	1.0266	1.1344	4.5427	14.7463	0.6081	1.3942
U - TF Full - Tx 10	0.5141	1.1427	1.0197	0.4471	3.3324	6.7136	0.3044	1.1107
U - TF Full - Tx 15	1.1672	1.9393	1.7379	1.0627	5.2127	8.3833	0.6100	1.0778
U - TF Full - Tx 20	2.2453	2.7004	2.0193	1.6054	17.8338	23.1891	1.5259	1.6881
U - TF Full - Tx 25	2.8828	3.5390	1.8255	1.6634	18.6052	23.9477	1.7422	1.9002
U - TF Low - Tx 5	0.2373	0.1982	2.2199	0.5600	4.1982	14.3756	0.0845	0.1632
U - TF Low - Tx 10	1.0028	1.9335	1.0553	0.4318	4.2247	6.9989	0.2904	0.5618
U - TF Low - Tx 15	1.3585	2.1160	1.6823	0.9205	5.6575	8.3117	0.5841	1.0287
U - TF Low - Tx 20	9.8762	10.5142	1.9202	1.4866	23.4170	17.0965	2.3873	1.1604
U - TF Low - Tx 25	10.7421	11.3821	1.7006	1.4891	25.1804	17.6147	2.6215	1.3378
H - TF Full - Tx 5	0.1357	0.8439	0.0056	0.0070	0.1657	0.4664	0.0717	0.0619
H - TF Full - Tx 10	0.1024	0.6649	0.0058	0.0068	0.1848	0.6357	0.0738	0.0920
H - TF Full - Tx 15	0.0354	0.0129	0.0055	0.0059	0.1347	0.0728	0.0654	0.0261
H - TF Full - Tx 20	0.0351	0.0119	0.0054	0.0057	0.1507	0.0760	0.0662	0.0259
H - TF Full - Tx 25	3.5212	4.8271	0.1136	0.1342	8.4600	9.6575	1.0805	1.1611
H - TF Low - Tx 5	0.0231	0.0147	0.0016	0.0023	0.0347	0.0224	0.0317	0.0248
H - TF Low - Tx 10	0.0555	0.0100	0.0197	0.0157	0.4826	0.3008	0.0444	0.0273
H - TF Low - Tx 15	3.1964	3.9478	1.3309	0.3157	36.9438	8.9894	2.1534	0.4793
H - TF Low - Tx 20	0.0267	0.0114	0.0023	0.0024	0.0926	0.0490	0.0354	0.0239
H - TF Low - Tx 25	4.5980	3.7901	0.2167	0.1288	14.8462	8.6025	1.7690	1.0210

1 is greater than that of the beam 2 (maximum approximately 20 dB). Since the vehicle UE leaves the main lobe of the BS once the overtaking process ends, the received power of all beams begins to decrease.

In most cases, the impact on the received power during the overtaking process due to the traffic flow is not significant. However, in the highway scenario, when the vehicle UE overtakes the bus (see Fig. 19 (a) and (b)), the fluctuations of received power under full traffic flow are less significant than those under low traffic flow. This is mainly because when the traffic flow is low, there is always a strong reflected ray from the random vehicles between snapshot 1 and snapshot 130, which results in small-scale fading significantly. When the traffic flow is high, randomly placed vehicles do not produce such a reflected ray. When the placement of the random vehicles changes, the results may be different.

2) VARIOUS BS HEIGHTS

Fig. 21 shows the received power for various BS heights. For all the cases, the blue, red, green, yellow, and black dotted lines represent the received power on the Rx at BS heights of 5 m, 10 m, 15 m, 20 m, and 25 m, respectively.

In the urban scenario, when the height of the BS is 5 m, the traffic flow has a significant influence on the received power of the Rx (represented in Fig. 21 (a) and (b) with the blue dotted line). In the case of low BS height, when the traffic flow is full, due to a large number of moving vehicles on the lane, there are many non-line-of-sight (NLOS) cases, resulting in severe fading of the received power. When the BS height is higher than 5 m, the NLOS cases due to traffic flow will decrease. However, as the BS height increases, multipath increases significantly, resulting in increased oscillation effects. For example, when the BS height is 25 m,

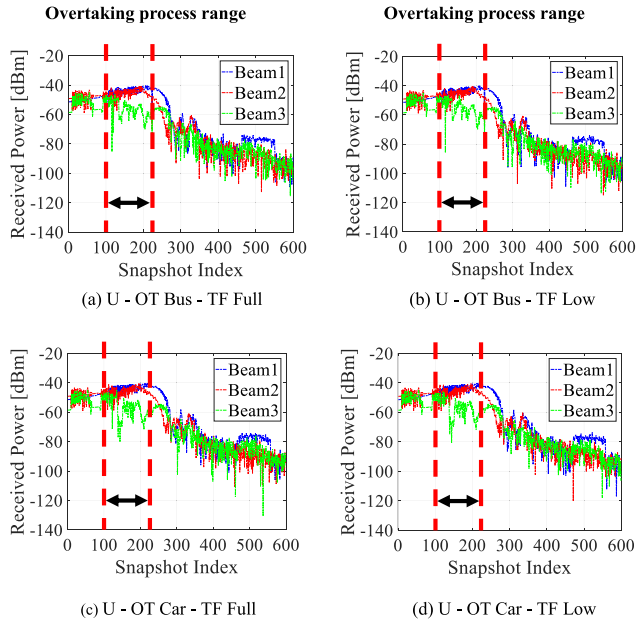


FIGURE 18. Received power of the overtaking situation in the urban scenario. (a) U - OT Bus - TF Full. (b) U - OT Bus - TF Low. (c) U - OT Car - TF Full. (d) U - OT Car - TF Low.

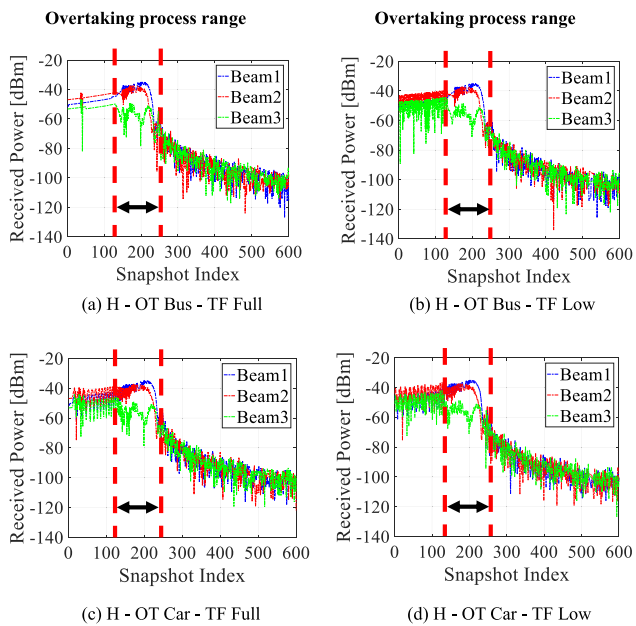


FIGURE 19. Received power of the overtaking situation in the highway scenario. (a) H - OT Bus - TF Full. (b) H - OT Bus - TF Low. (c) H - OT Car - TF Full. (d) H - OT Car - TF Low.

the oscillation effects are obvious and affected by the traffic flow.

In the highway scenario, different traffic flows have significant impacts on receiving power. Since the highway scenario is relatively simple, the impact of the moving vehicles on the received power is particularly significant compared to the complex urban scenario. For example, when the BS height is 25 m (black dotted line), the random moving scatterers on

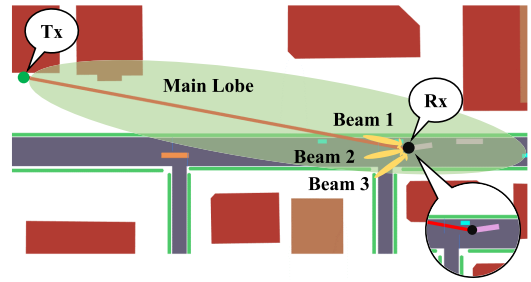


FIGURE 20. Schematic of the overtaking process.

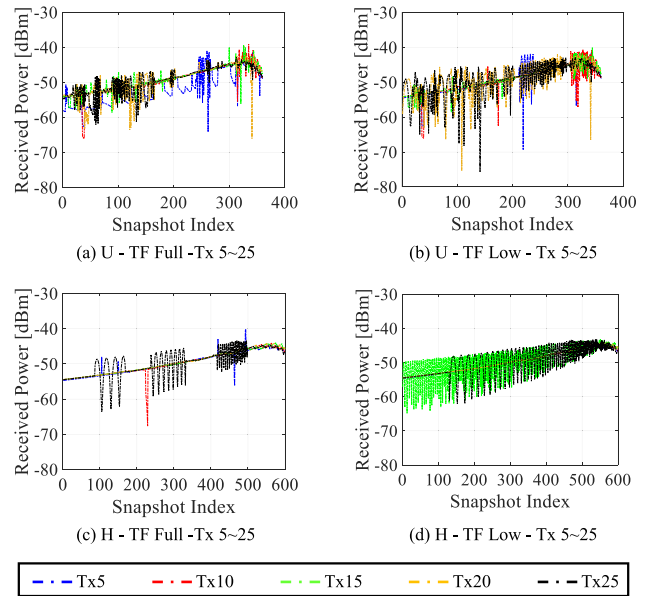


FIGURE 21. Received power of various BS heights. (a) U - TF Full - Tx 5~25. (b) U - TF Low - Tx 5~25. (c) H - TF Full - Tx 5~25. (d) H - TF Low - Tx 5~25.

the road will cause the significant small-scale fading, which can be mapped to the oscillation effects on the black dotted line. In addition, as shown in Fig. 21(d), when the BS height is 15 m (represented by the green dotted line), the significant small-scale fading is due to the metallic noise barrier on the roadside. The details are shown in Fig. 29(a).

In summary, the results indicate that when the BS is at the roadside, the vehicle UE can achieve more reliable communication by adopting beam switching during the overtaking process. When the BS height is relatively low (e.g., 5 m), the NLOS is likely to happen due to the blockage of the vehicles, thus the communication quality might be affected. In the urban scenario, the received power is mainly affected more by urban furniture than the moving vehicles, and in the highway scenario, it is more affected by the moving vehicles.

B. RMS DELAY SPREAD

RMS delay spread is used to quantify the dispersion effect of multipath channel. It is defined as the square root of the second central moment of the power delay

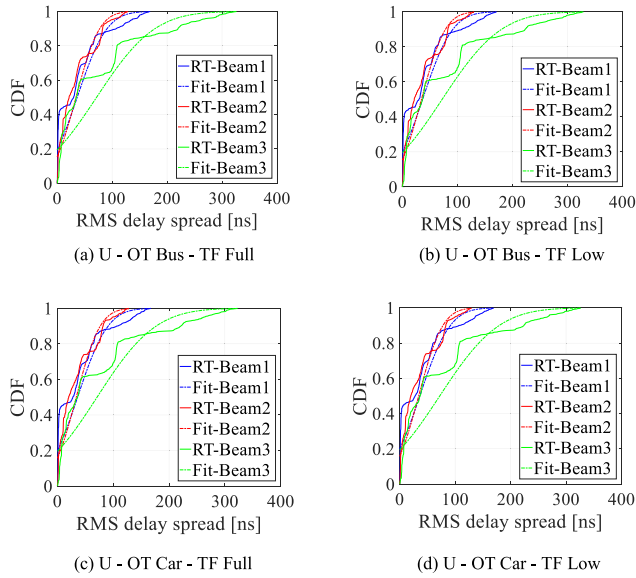


FIGURE 22. CDF of the DS of overtaking situation in the urban scenario. (a) U - OT Bus - TF Full. (b) U - OT Bus - TF Low. (c) U - OT Car - TF Full. (d) U - OT Car - TF Low.

profile (PDP) [45]:

$$\sigma_\tau = \sqrt{\frac{\sum_{n=1}^N \tau_n^2 \cdot P_n}{\sum_{n=1}^N P_n} - \left(\frac{\sum_{n=1}^N \tau_n \cdot P_n}{\sum_{n=1}^N P_n} \right)^2} \quad (2)$$

where σ_τ denotes the RMS delay spread, P_n and τ_n denote the power and the excess delay of the n -th multipath, respectively. The cumulative distribution functions (CDFs) of the RMS delay spreads σ_τ in the simulations are shown in Fig. 22 - Fig. 25 for the overtaking situation and various BS heights in urban and highway scenarios, respectively. The mean values and the standard deviations (STDs) of RMS delay spread for each case are listed in Table 6.

1) OVERTAKING SITUATION

As shown in Fig. 22 - Fig. 23, the μ_{DS} in the urban scenario is larger than the μ_{DS} in the highway scenario. The reason is that there are more multipath components in the complex urban scenario than in the simple highway scenario.

In the urban scenario, whether the vehicle UE overtakes the bus or the vehicle UE overtakes the passenger car, the μ_{DS} of the beam 3 is approximately 70 ns, which is much larger than the μ_{DS} of the beam 1 and the beam 2 (around 35 ns). It's found from the simulation results that there are a large number of reflected rays generated from the buildings along the lanes, which arrive in the main lobe of beam 3 (see Fig. 24).

In the highway scenario, the mean value of DS is mainly affected by traffic flow. When the traffic flow is low, the mean value of DS is relatively small (6-7 ns). When the traffic flow is full, the mean value of DS is relatively large (22-23 ns) because there are more multipath components from the moving vehicles.

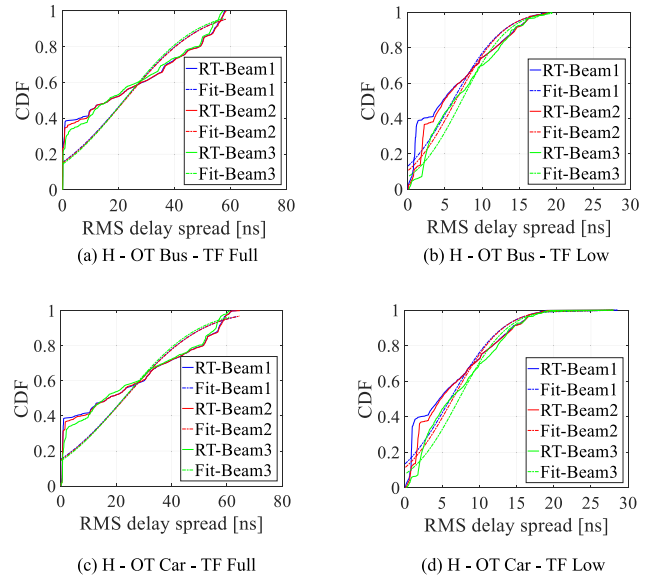


FIGURE 23. CDF of the DS of overtaking situation in the highway scenario. (a) H - OT Bus - TF Full. (b) H - OT Bus - TF Low. (c) H - OT Car - TF Full. (d) H - OT Car - TF Low.

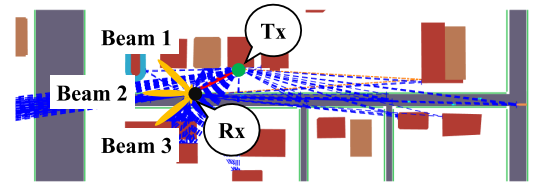


FIGURE 24. One simulation snapshot of the overtaking situation in the urban scenario.

2) VARIOUS BS HEIGHTS

From Fig. 25 and Table 6, we can see that in the urban scenario, when the BS height is 5 m, the mean value of DS is less than 4 ns. When the BS height is relatively high (e.g., higher than 5 m), a large number of multipath components result in larger mean value of DS, which is various from 20 ns to 36 ns.

However, in the highway scenario, the mean value of DS is not sensitive to the changes of BS height. No matter the BS height is 5 m or 25 m, the mean value of DS is less than 3 ns. Additionally, when the BS height is 15 m (represented with the green dotted line in Fig. 25(d)), the DS is relatively larger than other cases, the reason is that the influence of the metallic noise barrier on the roadside, which was mentioned before and the details are shown in Fig. 29(a).

C. RICIAN K-FACTOR

The Rician K -factor is a significant indicator of how the multipath components dominate the power contribution, which is defined as the ratio of the power of the strongest component to the power of the sum of the remaining components in the received signal [46]. The expression is shown as follows:

$$KF (dB) = 10 \cdot \log_{10} \left(\frac{P_{strongest}}{\sum P_{remaining}} \right) \quad (3)$$

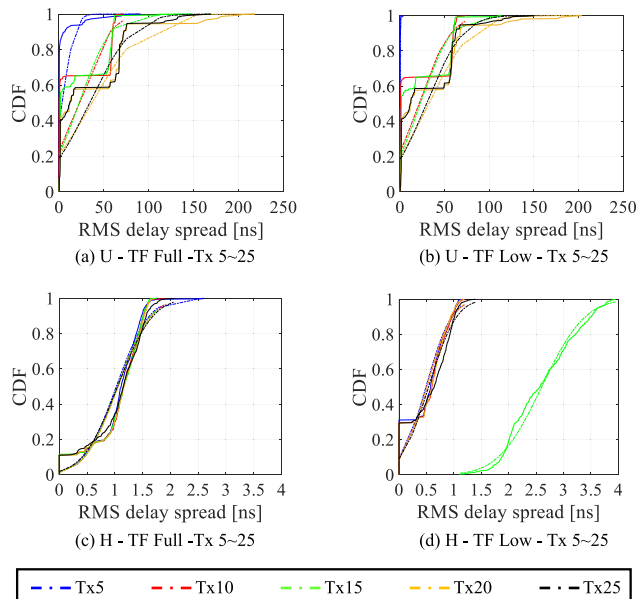


FIGURE 25. CDF of the DS of various BS heights. (a) U - TF Full - Tx 5~25. (b) U - TF Low - Tx 5~25. (c) H - TF Full - Tx 5~25. (d) H - TF Low - Tx 5~25.

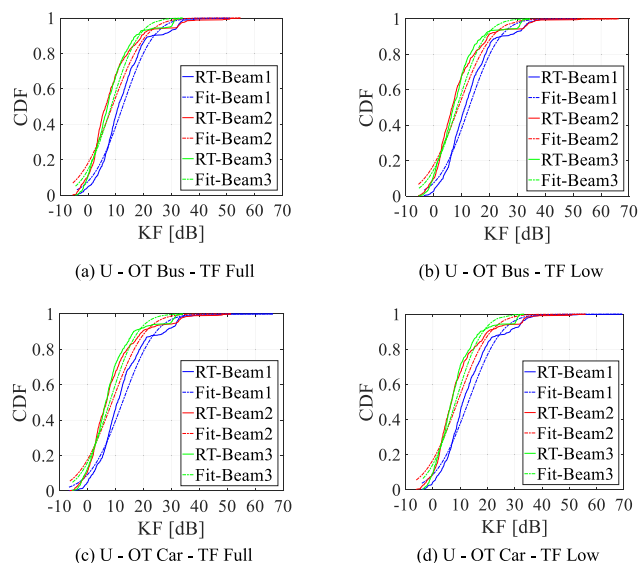


FIGURE 26. CDF of the KF of overtaking situation in the urban scenario. (a) U - OT Bus - TF Full. (b) U - OT Bus - TF Low. (c) U - OT Car - TF Full. (d) U - OT Car - TF Low.

where KF denotes the Rician K -factor, $P_{strongest}$ and $P_{remaining}$ denote the power of the strongest component and the power of each of the remaining components, respectively. The fitting results of Rician K -factor are summarized in Table 7 and the CDFs are compared in Fig. 26 - Fig. 28.

1) OVERTAKING SITUATION

Based on Fig. 26 and Fig. 27, the following conclusions are drawn: compared with the urban scenario, the line-of-sight (LOS) ray contributes the most to the received power in the highway scenario. Therefore, the μ_{KF} in the highway scenario (around 17 dB) is larger than μ_{KF} (around 10 dB) in the urban scenario.

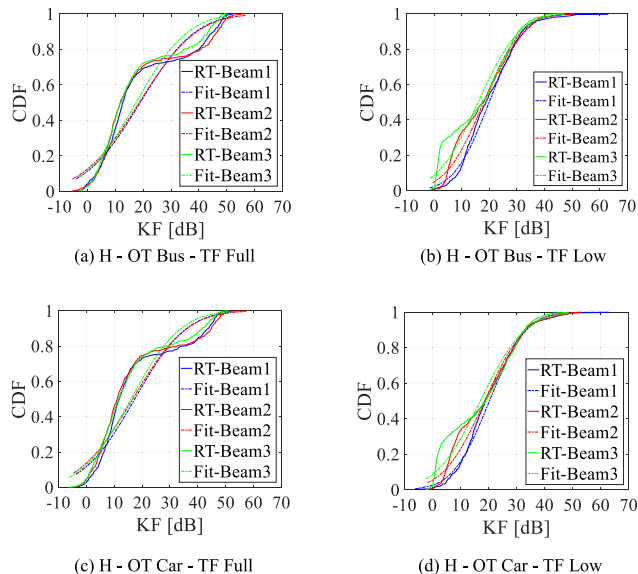


FIGURE 27. CDF of the KF of overtaking situation in the highway scenario. (a) H - OT Bus - TF Full. (b) H - OT Bus - TF Low. (c) H - OT Car - TF Full. (d) H - OT Car - TF Low.

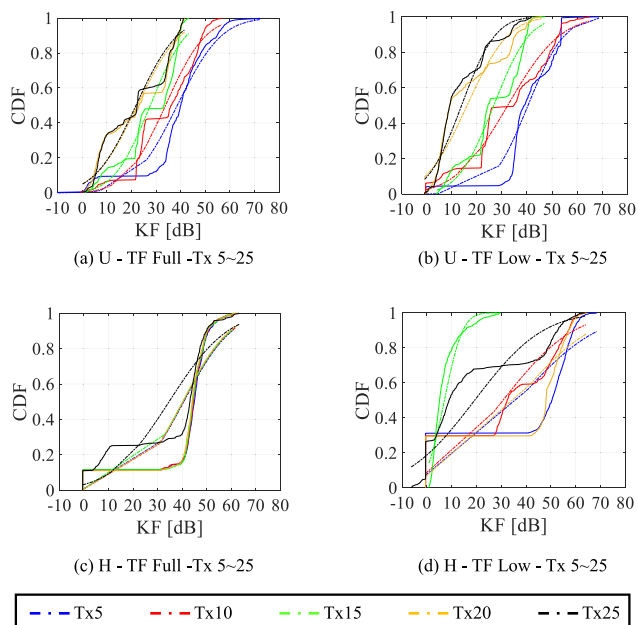


FIGURE 28. CDF of the KF of various BS heights. (a) U - TF Full - Tx 5~25. (b) U - TF Low - Tx 5~25. (c) H - TF Full - Tx 5~25. (d) H - TF Low - Tx 5~25.

2) VARIOUS BS HEIGHTS

Comparing Fig. 28 (a) with (b), we can find that in the urban scenario, as the height of the BS increases (various from 5 m to 25 m), the μ_{KF} gradually decreases from 40 dB to 15 dB (summarized in Table 7). This is because that the higher the BS, the more abundant multipath components in the urban scenario will occur, resulting in a gradual decrease in the μ_{KF} .

In the highway scenario, the μ_{KF} (around 35 dB) is not sensitive to the changes of the BS height (various from 5 m to 25 m). However, in the case “H - TF Low - Tx 15”, the μ_{KF} is relatively small (around 7 dB) due to the presence of a strong reflected ray from the metallic noise barrier (see Fig. 29).

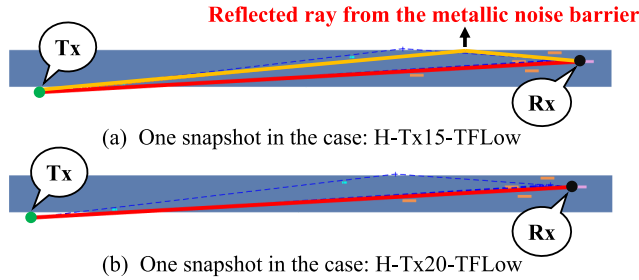


FIGURE 29. Simulation snapshots of various BS height in the highway scenario. (a) One snapshot in the case: H - Tx15 - TF Low. (b) One snapshot in the case: H - Tx20 - TF Low.

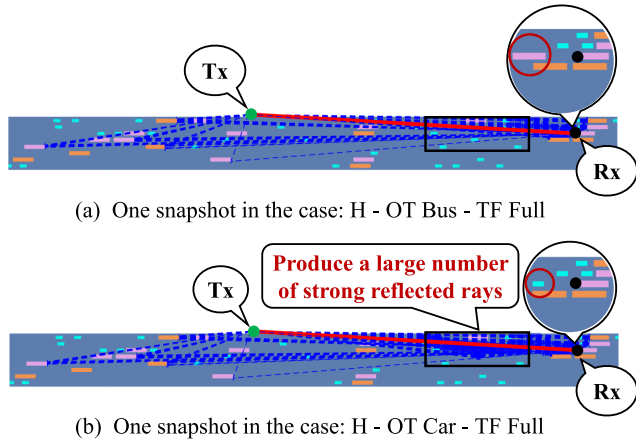


FIGURE 30. Simulation snapshots of different overtaking situations in the highway scenario. (a) One snapshot in the case: H - OT Bus - TF Full. (b) One snapshot in the case: H - OT Car - TF Full.

D. ANGULAR DOMAIN

Based on the 3GPP definition, the conventional angular spread calculation for the composite signal is given by

$$\sigma_{AS} = \sqrt{\frac{\sum_{n=1}^N (\theta_{n,\mu})^2 \cdot P_n}{\sum_{n=1}^N P_n}} \quad (4)$$

where σ_{AS} denotes the angular spread, P_n denotes the power of the n -th multipath, and $\theta_{n,\mu}$ is defined by:

$$\theta_{n,\mu} = \text{mod}(\theta_n - \mu_\theta + \pi, 2\pi) - \pi \quad (5)$$

μ_n is defined as:

$$\mu_\theta = \frac{\sum_{n=1}^N \theta_n \cdot P_n}{\sum_{n=1}^N P_n} \quad (6)$$

and θ_n is the angle of arrival/departure of the n -th multipath.

The angular spreads values for each case are summarized in Table 8.

1) OVERTAKING SITUATION

Generally speaking, for the overtaking situation in the urban scenario, the mean value of ASD and ASA (around 35° and 50° , respectively) are larger than ESD and ESA (around 15° and 23° , respectively), implying that most of the multipaths come from the horizontal direction. This truthfully reflects the fact that in the simulation results, a large number of reflected rays are mainly from the surface of buildings and the moving vehicle bodies.

In the highway scenario, under the condition of full traffic flow, the two situations of “vehicle UE overtaking the bus” and “vehicle UE overtaking car” are compared. We can find that when the vehicle UE overtakes the bus, both ASD and ASA are smaller than when the vehicle UE overtakes the car. The reason is that when the car is in front of the vehicle UE, since the height of the car is low (1.6 m) and the height of the vehicle UE is 3 m, more multipath components from the surrounding scatterers can get to Rx (see Fig. 30).

2) VARIOUS BS HEIGHTS

According to Table 8, we can find that in the urban scenario, the mean values of the horizontal angular spreads (ASD and ASA) increase with the height of the BS. In the highway scenario, it mainly depends on the condition of the moving vehicles.

V. CONCLUSION

In this paper, a comprehensive study on the channel characteristics of the V2I link in mmWave band (22.1-23.1 GHz) for various road environments and deployment configurations is conducted. In combination with the dynamic mobility pattern of the antenna on the RT simulator, mmWave channel characteristics for “overtaking situation” and “various BS height” in typical urban and highway scenarios are evaluated, respectively. By considering different traffic flows, multiple antennas and beam switching (Beam 1, 2, 3) at the vehicle UE, 44 cases have been considered in this work.

The key channel parameters in target scenarios are extracted and analyzed from the calibrated simulations. Based on the analysis of the channel parameters, a series of interesting findings in the V2I link are summarized as follows:

During the overtaking process, when the BS is beside the road, the received power of three beams in different directions has a difference of 10 dB. As the vehicle UE is further approaching the BS, the originally communicating beam on the vehicle UE (the beam which has the greatest received power before the overtaking process) will deviate from the main lobe of the BS. In this case, the received power of different beams may even differ by up to 20 dB, thus multiple antennas and beam switching can be effectively used to achieve more reliable communication of the V2I link.

In the urban scenario, the received power is mainly affected by the surrounding objects along the roadside, and in the highway scenario, it is more affected by the moving vehicles on the lane.

In the highway scenario, the mean value of DS is mainly affected by traffic flow. When the traffic flow is low, the mean value of DS is relatively small (6-7 ns). When the traffic flow is full, the mean value of DS is relatively large (22-23 ns), which is approximately three times the mean

value of DS with low traffic flow, because there are more multipath components generated from the moving vehicles.

For the various heights of the BS, we find that in the urban scenario, as the height of the BS increases, the type and number of multipath increase. Meanwhile the mean value of KF decreases and the mean values of DS increases. However, in the highway scenario, the mean values of KF and DS are not sensitive to the BS height. The mean value of the horizontal angular spreads (ASD and ASA) increase with the higher BS in the urban scenario. In the highway scenario, it mainly depends on the condition of the moving vehicles.

In summary, the analysis and the provided parameters in this paper will help the researchers understand the channel characteristics of the V2I link in mmWave band and support the link-level and system-level design for future vehicular communications.

REFERENCES

- X. Xu, Y. Liu, W. Wang, X. Zhao, Q. Z. Sheng, Z. Wang, and B. Shi, "ITS-frame: A framework for multi-aspect analysis in the field of intelligent transportation systems," *IEEE Trans. Intell. Transp. Syst.*, vol. 20, no. 8, pp. 2893–2902, Aug. 2019.
- I. Kabashkin, "Reliable v2x communications for safety-critical intelligent transport systems," in *Proc. Adv. Wireless Opt. Commun. (RTUWO)*, Nov. 2017, pp. 251–255.
- D. He, L. Wang, K. Guan, B. Ai, J. Kim, and Z. Zhong, "Channel characterization for mmwave vehicle-to-infrastructure communications in urban street environment," in *Proc. 13th Eur. Conf. Antennas Propag. (EuCAP)*, Mar. 2019, pp. 1–5.
- J.-Y. Hwang, M. Jung, and S.-W. Lee, "LTE based V2X receiver to support high speed," in *Proc. Int. Conf. Inf. Commun. Technol. Converg. (ICTC)*, Oct. 2017, pp. 747–749.
- Study on LTE-Based V2X Services (Release 14)*, document 36.885, 3GPP, Jun. 2016.
- A. Bazzi, B. M. Masini, A. Zanella, and I. Thibault, "On the performance of IEEE 802.11p and LTE-V2V for the cooperative awareness of connected vehicles," *IEEE Trans. Veh. Technol.*, vol. 66, no. 11, pp. 10419–10432, Nov. 2017.
- T. S. Rappaport, Y. Xing, G. R. MacCartney, A. F. Molisch, E. Mellios, and J. Zhang, "Overview of millimeter wave communications for fifth-generation (5G) wireless networks-with a focus on propagation models," *IEEE Trans. Antennas Propag.*, vol. 65, no. 12, pp. 6213–6230, Dec. 2017.
- C. Bila, F. Sivrikaya, M. A. Khan, and S. Albayrak, "Vehicles of the future: A survey of research on safety issues," *IEEE Trans. Intell. Transp. Syst.*, vol. 18, no. 5, pp. 1046–1065, May 2017.
- W. Wang, T. Jost, C. Gentner, S. Zhang, and A. Dammann, "A semiblind tracking algorithm for joint communication and ranging with OFDM signals," *IEEE Trans. Veh. Technol.*, vol. 65, no. 7, pp. 5237–5250, Jul. 2016.
- F.-L. Luo, "5G new radio (NR): Standard and technology," ZTE Corp., Shenzhen, China, Tech. Rep. S1 2017 and 57, 2017.
- A. Tassi, M. Egan, R. J. Piechocki, and A. Nix, "Modeling and design of millimeter-wave networks for highway vehicular communication," *IEEE Trans. Veh. Technol.*, vol. 66, no. 12, pp. 10676–10691, Dec. 2017.
- J. Choi, V. Va, N. Gonzalez-Prelcic, R. Daniels, C. R. Bhat, and R. W. Heath, Jr., "Millimeter-wave vehicular communication to support massive automotive sensing," *IEEE Commun. Mag.*, vol. 54, no. 12, pp. 160–167, Dec. 2016.
- J. Zhang, P. Tang, L. Tian, Z. Hu, T. Wang, and H. Wang, "6–100 GHz research progress and challenges from a channel perspective for fifth generation (5G) and future wireless communication," *Sci. China Inf. Sci.*, vol. 60, no. 8, p. 080, Jun. 2017.
- W. Wang, T. Jost, and U.-C. Fiebig, "A comparison of outdoor-to-indoor wideband propagation at S-band and C-band for ranging," *IEEE Trans. Veh. Technol.*, vol. 64, no. 10, pp. 4411–4421, Oct. 2015.
- Study on Enhancement of 3GPP Support for 5G V2X Services*, document TR 22.886, 3GPP, Dec. 2018.
- Study on Scenarios and Requirements for Next Generation Access Technologies*, document TR 38.913, 3GPP, Jul. 2018.
- Study on New Radio Access Technology Physical Layer Aspects*, document TR 38.802, 3GPP, Sep. 2017.
- Study on Evaluation Methodology of New Vehicle-to-Everything (V2X) Use Cases for LTE and NR (Release 15)*, document 37.885, 3GPP, Jun. 2018.
- P. Tang, J. Zhang, A. F. Molisch, P. J. Smith, M. Shafi, and L. Tian, "Estimation of the K-factor for temporal fading from single-snapshot wideband measurements," *IEEE Trans. Veh. Technol.*, vol. 68, no. 1, pp. 49–63, Jan. 2019.
- E. Ben-Dor, T. S. Rappaport, Y. Qiao, and S. J. Lauffenburger, "Millimeter-wave 60 GHz outdoor and vehicle AOA propagation measurements using a broadband channel sounder," in *Proc. IEEE Global Telecommun. Conf. - GLOBECOM*, Dec. 2011, pp. 1–6.
- A. Kato, K. Sato, M. Fujise, and S. Kawakami, "Propagation characteristics of 60-GHz millimeter waves for ITS inter-vehicle communications," *IEICE Trans. Commun.*, vol. 84, no. 9, pp. 2530–2539, 2001.
- T. Jost, W. Wang, and M. Walter, "A geometry-based channel model to simulate an Averaged-Power-Delay profile," *IEEE Trans. Antennas Propag.*, vol. 65, no. 9, pp. 4925–4930, Sep. 2017.
- Y. Li, X. Cheng, and N. Zhang, "Deterministic and stochastic simulators for non-isotropic V2V-MIMO wideband channels," *China Commun.*, vol. 15, no. 7, pp. 18–29, Jul. 2018.
- B. R. Epstein and D. L. Rhodes, "GPU-accelerated ray tracing for electromagnetic propagation analysis," in *Proc. IEEE Int. Conf. Wireless Inf. Technol. Syst.*, Aug. 2010, pp. 1–4.
- J. Zhang, C. Pan, F. Pei, G. Liu, and X. Cheng, "Three-dimensional fading channel models: A survey of elevation angle research," *IEEE Commun. Mag.*, vol. 52, no. 6, pp. 218–226, Jun. 2014.
- C. Gentner, T. Jost, W. Wang, S. Zhang, A. Dammann, and U.-C. Fiebig, "Multipath assisted positioning with simultaneous localization and mapping," *IEEE Trans. Wireless Commun.*, vol. 15, no. 9, pp. 6104–6117, Sep. 2016.
- C.-F. Yang, B.-C. Wu, and C.-J. Ko, "A ray-tracing method for modeling indoor wave propagation and penetration," *IEEE Trans. Antennas Propag.*, vol. 46, no. 6, pp. 907–919, Jun. 1998.
- IEEE Standard for High Data Rate Wireless Multi-Media Networks*, IEEE, Piscataway, NJ, USA, 2017.
- W. Fan, I. Carton, P. Kyosti, and G. F. Pedersen, "Emulating ray-tracing channels in multiprobe anechoic chamber setups for virtual drive testing," *IEEE Trans. Antennas Propag.*, vol. 64, no. 2, pp. 730–739, Feb. 2016.
- D. He, B. Ai, M. Schmieder, Z. Zhong, J. Kim, B. Hui, H. Chung, I. Kim, and Y. Hao, "Influence analysis of typical objects in rural railway environments at 28 GHz," *IEEE Trans. Veh. Technol.*, vol. 68, no. 3, pp. 2066–2076, Mar. 2019.
- W. Wang, T. Jost, and U.-C. Fiebig, "An extended GSCM for mobile radio based positioning in outdoor-to-indoor environment," in *Proc. 21th URSI Gen. Assem. Sci. Symp. (URSI GASS)*, Aug. 2014, pp. 1–4.
- D. He, B. Ai, K. Guan, Z. Zhong, B. Hui, J. Kim, H. Chung, and I. Kim, "Channel measurement, simulation, and analysis for high-speed railway communications in 5G millimeter-wave band," *IEEE Trans. Intell. Transp. Syst.*, vol. 19, no. 10, pp. 3144–3158, Oct. 2018.
- D. He, B. Ai, K. Guan, L. Wang, Z. Zhong, and T. Kurner, "The design and applications of high-performance ray-tracing simulation platform for 5G and beyond wireless communications: A tutorial," *IEEE Commun. Surveys Tuts.*, vol. 21, no. 1, pp. 10–27, 1st Quart., 2019.
- J. O. Nielsen, W. Fan, P. C. F. Eggers, and G. F. Pedersen, "A channel sounder for massive MIMO and MmWave channels," *IEEE Commun. Mag.*, vol. 56, no. 12, pp. 67–73, Dec. 2018.
- A. W. Mbugua, W. Fan, Y. Ji, and G. F. Pedersen, "Millimeter wave multi-user performance evaluation based on measured channels with virtual antenna array channel sounder," *Ieee Access*, vol. 6, pp. 12318–12326, 2018.
- C. Zheng, Z. Xu, D. He, K. Guan, B. Ai, and J. M. Garcia-Loygorri, "Millimeter-wave channel measurement based ray-tracing calibration and analysis in metro," in *Proc. IEEE Int. Symp. Antennas Propag. USNC-URSI Radio Sci. Meeting*, Jul. 2019, pp. 1–2.
- K. Guan, D. He, B. Ai, B. Peng, A. Hrovat, J. Kim, Z. Zhong, and T. Kurner, "Millimeter-wave communications for smart rail mobility: From channel modeling to prototyping," in *Proc. IEEE Int. Conf. Commun. Workshops (ICC Workshops)*, May 2019, pp. 1–6.
- E. Zochmann, M. Hofer, M. Lerch, S. Pratschner, L. Bernado, J. Blumenstein, S. Caban, S. Sangodoyin, H. Groll, T. Zemen, A. Prokes, M. Rupp, A. F. Molisch, and C. F. Mecklenbrauker, "Position-specific statistics of 60 GHz vehicular channels during overtaking," *IEEE Access*, vol. 7, pp. 14216–14232, 2019.
- J. Blumenstein, S. Sangodoyin, A. Molisch, A. Prokes, J. Vychodil, T. Mikulasek, E. Zochmann, H. Groll, C. F. Mecklenbrauker, M. Hofer, and T. Zemen, "Vehicle-to-vehicle millimeter-wave channel measurements at 56–64 GHz," in *Proc. IEEE 90th Veh. Technol. Conf. (VTC-Fall)*, Sep. 2019, pp. 1–5.

- [40] F. Wang and K. Sarabandi, "An enhanced millimeter-wave foliage propagation model," *IEEE Trans. Antennas Propag.*, vol. 53, no. 7, pp. 2138–2145, Jul. 2005.
- [41] H. M. Rahim, C. Y. Leow, and T. A. Rahman, "Millimeter wave propagation through foliage: Comparison of models," in *Proc. IEEE 12th Malaysia Int. Conf. Commun. (MICC)*, Nov. 2015, pp. 236–240.
- [42] K. Guan, B. Ai, B. Peng, D. He, G. Li, J. Yang, Z. Zhong, and T. Kurner, "Towards realistic high-speed train channels at 5G millimeter-wave band—Part I: Paradigm, significance analysis, and scenario reconstruction," *IEEE Trans. Veh. Technol.*, vol. 67, no. 10, pp. 9112–9128, Oct. 2018.
- [43] K. Guan, B. Ai, B. Peng, D. He, G. Li, J. Yang, Z. Zhong, and T. Kurner, "Towards realistic high-speed train channels at 5G millimeter-wave band—Part II: Case study for paradigm implementation," *IEEE Trans. Veh. Technol.*, vol. 67, no. 10, pp. 9129–9144, Oct. 2018.
- [44] V. Degli-Esposti, F. Fuschini, E. M. Vitucci, and G. Falciasecca, "Measurement and modelling of scattering from buildings," *IEEE Trans. Antennas Propag.*, vol. 55, no. 1, pp. 143–153, Jan. 2007.
- [45] T. Rappaport, *Wireless Communications: Principles and Practice*, 22nd ed. Upper Saddle River, NJ, USA: Prentice-Hall, 2002.
- [46] L. Bernado, T. Zemen, F. Tufvesson, A. F. Molisch, and C. F. Mecklenbrauker, "Time- and frequency-varying K -factor of non-stationary vehicular channels for safety-relevant scenarios," *IEEE Trans. Intell. Transp. Syst.*, vol. 16, no. 2, pp. 1007–1017, Apr. 2015.



DONG YAN (Student Member, IEEE) received the B.E. degree in electrical engineering from Xidian University, in 2015, and the M.Sc. degree from Technische Universität Braunschweig, Braunschweig, Germany, in 2018. He is currently pursuing the Ph.D. degree with Beijing Jiaotong University, Beijing, China. His research activities are mainly in the millimeter-wave communications and vehicle-to-everything communications.



KE GUAN (Senior Member, IEEE) received the B.E. and Ph.D. degrees from Beijing Jiaotong University, in 2006 and 2014, respectively. In 2009, he was a Visiting Scholar with the Universidad Politécnica de Madrid, Spain. From 2011 to 2013, he was a Research Scholar with the Institut für Nachrichtentechnik (IfN), Technische Universität Braunschweig, Germany. From September 2013 to January 2014, he was invited to conduct joint research in the Universidad Politécnica de Madrid, Spain. In 2015, he received a Humboldt Research Fellowship for Postdoctoral Researchers. He is currently a Professor with the State Key Laboratory of Rail Traffic Control and Safety, School of Electronic and Information Engineering, Beijing Jiaotong University. He has authored or coauthored two books and one book chapter, more than 200 journals and conference papers, and four patents. His current research interests include measurement and modeling of wireless propagation channels, high-speed railway communications, vehicle-to-x channel characterization, and indoor channel characterization for high-speed short-range systems including future terahertz communication systems.

Dr. Guan is the Pole Leader of the European Railway Research Network of Excellence (EURNEX). He was a recipient of the 2014 International Union of Radio Science (URSI) Young Scientist Award. His articles received eight Best Paper Awards, including the IEEE Vehicular Technology Society 2019 Neal Shepherd Memorial Best Propagation Paper Award. He serves as a Publicity Chair for PIMRC, 2016, the Publicity Co-Chair for ITST, 2018, the Track Co-Chair for EuCNC, the Session Convener for EuCAP, from 2015 to 2019, and a TPC Member for many IEEE conferences, such as Globecom, ICC, and VTC. He is an Editor of IEEE ACCESS, the *IET Microwave, Antenna and Propagation*, and *Physical Communication*, and a Guest Editor of the IEEE TRANSACTIONS ON VEHICULAR TECHNOLOGY and the *IEEE Communication Magazine*. He has been a Delegate in 3GPP and a member of the IC1004 and CA15104 initiatives.



DANPING HE (Member, IEEE) received the B.E. degree from the Huazhong University of Science and Technology, in 2008, the M.Sc. degree from the Université Catholique de Louvain (UCL) and the Politecnico di Torino (PdT), in 2010, and the Ph.D. degree from the Universidad Politécnica de Madrid, in 2014.

In 2012, she was a Visiting Scholar with the Institut national de recherche en informatique et en automatique, France. She worked in Huawei Technologies, from 2014 to 2015, as a Research Engineer. From 2016 to 2018, she conducted a Postdoctoral Research in Beijing Jiaotong University, where she is currently an Associate Professor. She has authored or coauthored more than 40 articles, three patents, and one IEEE standard. Her articles received five Best Paper Awards and she received the 2019 Applied Computational Electromagnetics Society (ACES)—China Young Scientist Award. Her current research interests include radio propagation and channel modeling, ray-tracing technologies, and wireless communication algorithm design.



BO AI (Senior Member, IEEE) received the master's and Ph.D. degrees from Xidian University, China. He graduated from Tsinghua University with the honor of Excellent Postdoctoral Research Fellow in 2007. He was a Visiting Professor with the Electrical Engineering Department, Stanford University, in 2015. He is currently working at Beijing Jiaotong University (BJTU) as a Full Professor and a Ph.D. Candidate Advisor. He has authored or coauthored eight books and published

more than 300 academic research articles in his research area. He holds 26 invention patents. He has been the research team leader for 26 national projects and received some important scientific research prizes. He has been notified by the Council of Canadian Academies (CCA) that, based on the Scopus database, he has been listed as one of the Top 1% of authors in his field all over the world. His interests include the research and applications of channel measurement and channel modeling, and dedicated mobile communications for rail traffic systems. He is an IET Fellow and an IEEE VTS Distinguished Lecturer. He has received many awards such as the Outstanding Youth Foundation from the National Natural Science Foundation of China, the Qishi Outstanding Youth Award by the Hong Kong Qishi Foundation, the New Century Talents by the Chinese Ministry of Education, the Zhan Tianyu Railway Science and Technology Award of the Chinese Ministry of Railways, and the Science and Technology New Star of the Beijing Municipal Science and Technology Commission. He has been a Co-Chair or a Session/Track Chair for many international conferences. He is an Editor of the IEEE TRANSACTIONS ON CONSUMER ELECTRONICS and an Editorial Committee Member of the *Wireless Personal Communications* journal. He has been the Lead Guest Editor for Special Issues of the IEEE TRANSACTIONS ON VEHICULAR TECHNOLOGY, the IEEE ANTENNAS AND PROPAGATIONS LETTERS, and the *International Journal on Antennas and Propagation*.



ZAN LI is currently pursuing the bachelor's degree with Beijing Jiaotong University, Beijing, China. His research interests include millimeter-wave communications and vehicle-to-everything communication.



JUNHYEONG KIM received the B.E. degree from the Department of Electronic Engineering, Tsinghua University, Beijing, China, in 2008, and the M.S. and Ph.D. degrees from the School of Electrical Engineering, Korea Advanced Institute of Science and Technology (KAIST), Daejeon, South Korea, in 2011 and 2020, respectively. Since 2011, he has been with the Electronics and Telecommunications Research Institute (ETRI), where he is taking part in the development of mmWave-band vehicular communication systems, and has been involved in the 5G new radio standardization in 3GPP RAN1 Working Group as a Delegate at ETRI since August 2017. His main research interests include millimeter-wave communications, vehicular communications, cooperative communications, and handover.



HEESANG CHUNG received the B.S. degree in physics from the Korea Advanced Institute of Science and Technology, Daejeon, South Korea, in 1993, and the M.S. and Ph.D. degrees from Chungnam National University, in 1995 and 1999, respectively. Since 1999, he has been with the Electronics and Telecommunications Research Institute (ETRI), where he is currently the Principal Researcher. His career at ETRI began with optical communications, and moved on to mobile and wireless communication systems in 2005. He was involved in research projects related to LTE and LTE-Advanced from 2006 to 2010. His recent research interests are in 5G with a special emphasis on high data-rate services for passengers on public transportation, such as the buses, subway, and bullet trains.



ZHANGDAI ZHONG (Senior Member, IEEE) is currently a Professor and Advisor of Ph.D. candidates with Beijing Jiaotong University, Beijing, China. He is also the Director with the School of Computer and Information Technology and a Chief Scientist with the State Key Laboratory of Rail Traffic Control and Safety, Beijing Jiaotong University. He is also the Director of the Innovative Research Team, Ministry of Education, and a Chief Scientist of the Ministry of Railways in China. He is an Executive Council Member of the Radio Association of China and the Deputy Director of the Radio Association of Beijing. He has authored or coauthored seven books, five invention patents, and more than 200 scientific research articles in his research area. His research interests include wireless communications for railways, control theory and techniques for railways, and GSM-R systems. His research has been widely used in the railway engineering, such as Qinghai-Xizang Railway, Datong-Qinhuangdao Heavy Haul railway, and many high-speed railway lines of China. He received the Mao Yisheng Scientific Award of China, the Zhan Tianyou Railway Honorary Award of China, and the Top Ten Science/Technology Achievements Award of Chinese Universities.

...